European Journal of Remote Sensing - 2014, 47: 643-654
doi: 10.5721/EuJRS20144736
Received 16/04/2014, accepted 11/07/2014

**European Journal of Remote Sensing**
An official journal of the Italian Society of Remote Sensing

www.aitjournal.com

# A contrast-sensitive Potts model custom-designed for change detection

**Ming Hao[1], Wenzhong Shi[2*], Kazhong Deng[1] and Hua Zhang[1]**

[1]School of Environment Science and Spatial Informatics,
China University of Mining and Technology, 1 Daxue Road, 221116 - Xuzhou, China
[2]Joint Research Laboratory on Spatial Information, The Hong Kong Polytechnic University
and Wuhan University, 999077 and 430079 - Hong Kong and Wuhan, China
*Corresponding author, e-mail address: lswzshi@polyu.edu.hk

## Abstract
A contrast-sensitive Potts model (CSP) custom-designed for change detection is presented using remotely sensed images. In traditional Potts model, a constant penalty coefficient is used, which results in ignorance of significant details and excessively homogenous patches during change detection using the difference image generated from multitemporal images. In the proposed CSP, the difference image is divided into unchanged, uncertainty and changed regions. Then different linear functions are introduced instead of the constant penalty coefficient for different regions. Two experiments were carried on optical satellite images, and the results indicate that the proposed CSP produces more accurate change maps than some state-of-the-art methods.

**Keywords:** Contrast-sensitive, Potts model, change detection, remotely sensed images.

## Introduction
In recent years, change detection has been one of the important research issues in remote sensing. Change detection aims to detect changes occurred on the Earth surface by analyzing multitemporal images acquired at different times on the same geographical area [Bruzzone and Bovolo, 2013; Hao et al., 2014], which is widely implemented to fire damage assessment [Mari et al., 2012], collapsed building detection due to earthquake [Shi and Hao, 2013], monitoring of forest recovery [Chen et al., 2014], and so on.

The change detection technique could be categorized as either supervised or unsupervised according to the nature of data processing and results [Du et al., 2012]. Initially unsupervised ones detect changes by comparing the multitemporal images pixel by pixel, such as image differencing, image ratio, image regression and change vector analysis (CVA), etc. [Bruzzone and Prieto, 2000; Zhang et al., 2014]. Thanks to the simple work, the image differencing method is widely used. In the past decades, more methods were proposed to fuse spatial and spectral information based on the difference image generated by image differencing or CVA, especially the Markov random field (MRF). The Potts model is one

of often used models in MRF to describe the spatial relationships for a current pixel in the difference image [Bruzzone and Prieto, 2000; Xiong et al., 2012]. However, in the traditional Potts model, a constant penalty coefficient is used and an over-smooth change map will be eventually brought without well defining for specific pixels (i.e. pixels having high probabilities belonging to one class) [Tso and Olsen, 2005], in which significant details (i.e. edge information) may be ignored and excessively homogenous patches may be obtained. The edge information was integrated into the spatial energy function of MRF to preserve small structures and edges [Ghosh et al., 2012; Tarabalka et al., 2010] for classification and object detection. Especially for change detection, it is necessary to find a custom-designed Potts model of MRF to improve this shortness, because pixels in the difference image have different probabilities belonging to changed or unchanged parts and a constant penalty for all pixels cannot exploit the spatial information appropriately.

In this paper, a contrast-sensitive Potts model custom-designed for change detection is proposed to reduce the over-smooth risk to a certain extent. The custom-designed Potts model contributes to find the suitable penalty coefficients of the spatial contribution for each pixel in the difference image during the change detection process.

## Proposed contrast-sensitive Potts model for change detection approach

Generally, Let $\mathbf{X}_1 = \{X_1(i,j) \mid 1 \le i \le H, 1 \le j \le W\}$ and $\mathbf{X}_2 = \{X_2(i,j) \mid 1 \le i \le H, 1 \le j \le W\}$ be two temporal images acquired from the same geographical area at two different times, $t_1$ and $t_2$. Since the focus is on the change detection process, it is assumed that the images have been co-registered and radiometrically corrected. Then the difference image $\mathbf{X} = \{X(i,j) \mid 1 \le i \le H, 1 \le j \le W\}$ is generated using CVA method [Chen et al., 2003].

### *Change detection using MRF*

Suppose the difference image $\mathbf{X}$ is given, and $\mathbf{L} = \{\mathbf{L}_l, l = 1,2,...,2^{HW}\}$ is all the possible sets of labels for the difference image $\mathbf{X}$, where $\mathbf{L}_l = \{L_l(i,j), 1 \le i \le H, 1 \le j \le W\}$ is a generate set of labels in the difference image $\mathbf{X}$, and $L_l(i,j)$ belongs to unchanged and changed classes. The Maximum a Posteriori (MAP) is adopted to produce a set $\mathbf{L}^*$ of the labels that maximizes the following equation:

$$\mathbf{L}_k = \arg\max_{\mathbf{L}_l \in \mathbf{L}} \{P(\mathbf{L}_l)\, p(\mathbf{X} \mid \mathbf{L}_l)\} \quad [1]$$

where $P(\mathbf{L}_l)$ is a priori probability distribution of the class labels of the difference image, and $p(\mathbf{X}|\mathbf{L}_l)$ is a conditional probability density function of the pixel values in the difference image. In terms of the MRF approach, maximizing the posterior probability as equation [1] is equivalent to minimize the following energy $U_{\mathrm{MRF}}(X(i,j))$ with a pixel *X(i,j)* [Bruzzone and Prieto, 2000; Tarabalka et al., 2010]:

$$U_{\mathrm{MRF}}(X(i,j)) = U_{\mathrm{spectral}}(X(i,j)) + U_{\mathrm{spatial}}(X(i,j)) \quad [2]$$

where $U_{\mathrm{spectral}}(X(i,j))$ and $U_{\mathrm{spatial}}(X(i,j))$ denote the spectral and spatial energy function from the difference image, respectively.

The detailed spectral energy term can be written as

$$U_{\text{spectral}}\left(X(i,j)\right)=\frac{1}{2}ln\left|2\pi\sigma_k^2\right|+\frac{1}{2}\left(X(i,j)-\mu_k\right)^2\left(\sigma_k^2\right)^{-1} \quad [3]$$

where $\mu_k$ and $\sigma_k^2$ denote the mean and variance of class $k$ (unchanged or changed), respectively.
The spatial energy of the pixel $X(i,j)$ is defined as

$$U_{\text{spatial}}\left(X(i,j)\right)=\sum_{(g,h)\in N(i,j)} I\left(L_l(i,j),L_l(g,h)\right) \quad [4]$$

where N($i,j$) denotes the local neighborhood (i.e. 3×3 windows used in this paper) of the pixel $X(i,j)$, and $I$ is the Potts model defined as formula [5], $\beta > 0$ is a penalty coefficient value fixed by the user to tune the influence of the spatial contextual information.

$$I\left(L_l(i,j),L_l(g,h)\right)=\begin{cases}-\beta & L_l(i,j)=L_l(g,h)\\ 0 & L_l(i,j)\neq L_l(g,h)\end{cases} \quad [5]$$

***The contrast-sensitive Potts model***

First, considering the ranges of pixel values of the difference image belonging to the changed and unchanged generally have overlap, the difference image is divided into unchanged region, uncertainty region and changed region using two thresholds $T_1$ and $T_2$ as shown in Figure 1 by two thresholds $T_1$ and $T_2$. In order to obtain $T_1$ and $T_2$, the fuzzy c-means (FCM) method [Bezdek et al., 1984] is adopted and implemented to the difference image to preliminarily partition the pixels into unchanged and changed clusters. Suppose there are $n$ pixels in the difference image $\mathbf{X}=\{x_1, x_2,\ldots, x_n\}$, and $c$ is the number of the clusters. The FCM aims at obtaining membership probability $u_{ij}\in[0,1]$ ($\sum_{i=1}^{c}u_{ij}=1\,(j=1,2,...,n)$) of the pixel $x_j$ in the difference image for the $i^{\text{th}}$ cluster by minimizing the objective function

$$J(\mathbf{U},\mathbf{V})=\sum_{i=1}^{c}\sum_{j=1}^{n}u_{ij}^{m}\left\|x_j-v_i\right\|^2 \quad [6]$$

where $\mathbf{U}=[u_{ij}]$ is the membership probability matrix of $\mathbf{X}$, $\mathbf{V}=[v_1,v_2,\ldots,v_c]$ is the matrix composed of $c$ central values, each one containing the coordinates of a cluster centre, and $m$ is a weighting exponent and usually set to 2, a widely used value in many works. Finally, the initial change map, the membership probability $\mathbf{U}$ of pixels and the central values of unchanged and changed parts $C_1$ and $C_2$ in the difference image are achieved.
Then the values of $T_1$ and $T_2$ can be obtained using the following equation:

$$\begin{cases}T_1=M_{\text{mid}}-\alpha_1\left(M_{\text{mid}}-C_1\right)\\ T_2=M_{\text{mid}}+\alpha_2\left(C_2-M_{\text{mid}}\right)\end{cases} \quad [7]$$

where $M_{\text{mid}}$ is the middle pixel, which has same probability belonging to unchanged and changed clusters in the FCM process, $C_1$ and $C_2$ are the central pixels of unchanged and changed clusters and calculated in the FCM process (as shown in Fig. 1), $\alpha_1$ and $\alpha_2$ are constants tuning the range of uncertainty region.

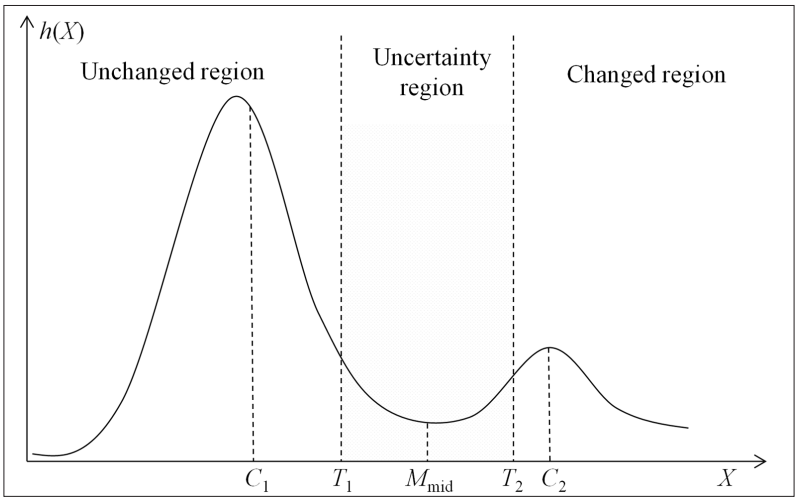


**Figure 1 - Unchanged, uncertainty and changed regions in the difference image.**

Then three strategies are introduced for different regions to obtain the contrast penalty coefficient $\beta_{\text{m}}$ of Potts model, and the detailed function is presented as follows

$$\beta_m\left(X(i,j)\right)=\begin{cases}\beta\dfrac{X(i,j)-X_{\min}}{T_1-X_{\min}} & X(i,j)<T_1\\ \beta & T_1\le X(i,j)\le T_2\\ \beta\dfrac{X_{\max}-X(i,j)}{X_{\max}-T_2} & X(i,j)>T_2\end{cases} \quad [8]$$

where $X_{\min}$ and $X_{\max}$ are gray values of the minimum and maximum pixels in the difference image, respectively. Therefore, the contrast penalty coefficient $\beta_{\text{m}}$ replaces the constant $\beta$ and the contrast-sensitive Potts model is obtained.

In this condition, when the gray value of pixel is smaller than $T_1$, the penalty coefficient $\beta_{\text{m}}$ linearly decreases with the gray value of pixels ranging from $T_1$ to the $X_{\min}$. Namely, the influence of the spatial contextual information reduces for pixels with smaller gray values considering these pixels has larger probabilities belonging to the unchanged part. When the gray value of pixel is larger than $T_2$, the penalty coefficient drops with the gray value of pixels increasing form $T_2$ to $X_{\max}$. Thus, the influence of spatial information is also reduced for the pixels with larger gray values due to their larger probabilities belonging to the changed part. Otherwise, a constant weighting coefficient is adopted for the pixels in the uncertainty region, and the spatial information is exploited to refine the initial change map.

The contribution of CSP is that a contrast penalty coefficient is employed based on the gray value of pixels to tune the spatial energy properly, which reduces the risk of over-smooth results and losing significant details to a certain extent.

Finally, MRF with contrast-sensitive Potts model is performed to refine the initial change map after the contrast penalty coefficient $\beta_m$ is determined. There are some iterative algorithms to minimize MRF, such as simulated annealing (SA), maximum a posterior margin (MPM) and iteration condition model (ICM) [Solberg et al., 1996]. Considering the computational complexity, ICM is adopted in this paper to minimize MRF.

The implementation of CSP mainly includes three steps as Figure 2:

- Step 1: Unsupervised change detection using FCM method. The difference image is obtained used CVA method. Then FCM method is implemented to the difference image and clusters the pixels into unchanged and changed parts. The change map and cluster center of the both parts generated by FCM are used as the initial result and parameters of CSP, respectively;
- Step 2: Computation of the contrast penalty coefficient. The two thresholds $T_1$ and $T_2$ are calculated based on results in Step 1 and divide the difference image to unchanged, uncertainty and changed regions. Then the contrast penalty coefficient is computed using equation [8];
- Step 3: Unsupervised change detection using the contrast-sensitive Potts model. After obtaining the contrast penalty coefficients, MRF with contrast-sensitive Potts model is run to refine the initial change map yielded by FCM in Step 1. Finally, the change detection result is obtained through minimizing the energy equation [2] using the ICM algorithm.

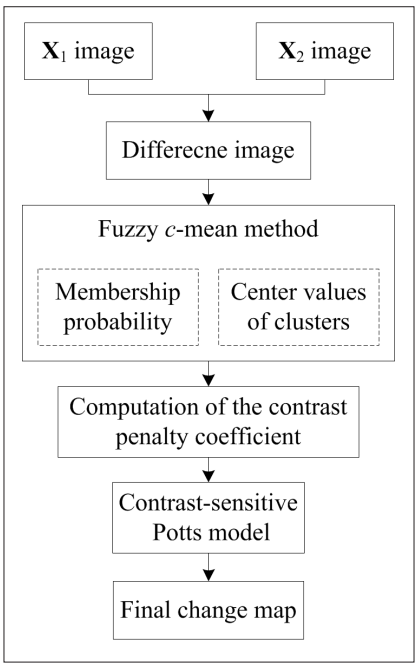


**Figure 2 - Flowchart of the proposed method.**

## Experimental results and discussion

Two experiments were conducted to test the performance of CSP. Comparisons were made between CSP, the multiresolution level set (MLS), MLS with Kittler algorithm (MLSK) [Bazi et al., 2010], FCM, the combination of expectation maximization (EM) and MRF [Bruzzone and Prieto, 2000], and the combination of FCM and MRF. Three indices are used to evaluate the results: 1) miss detection (*MD*): the number of changed pixels incorrectly classified as unchanged. The miss detection rate $P_{\mathrm{m}}$ is calculated by the ratio $P_{\mathrm{m}} = MD/N_0 \times 100\%$, here $N_0$ is the total number of changed pixels counted in the ground reference map; 2) false alarm (*FA*): the number of unchanged pixels wrongly detected as changed. The false detection rate $P_{\mathrm{f}}$ is described by the ratio $P_{\mathrm{f}} = FA/N_1 \times 100\%$, where $N_1$ is the total number of unchanged pixels counted in the ground reference map; 3) total error (*TE*): the total number of detection error including both miss and false detection, which is the sum of the *MD* and the *FA*. Hence, the total error rate $P_{\mathrm{t}}$ is described using $P_{\mathrm{t}} = (FA + MD)/(N_0 + N_1) \times 100\%$.

### *Experiment on the data set 1*

In the first experiment, the two temporal images (300×280 pixels) were used, which were acquired by the Landsat 7 Enhanced Thematic Mapper Plus (ETM+) sensor in August 2001 ($t_1$) and August 2002 ($t_2$) in the Northeast of China. Figure 3a and 3b show the band 4 of the both images, respectively. The $t_1$ image was registered and radiometrically corrected (i.e. histogram matching) to the $t_2$ image. Then the difference image was generated with bands 1, 2, 3, 4, 5 and 7 using CVA method. Moreover, the ground reference map of changes was produced manually and shown in Figure 3c.

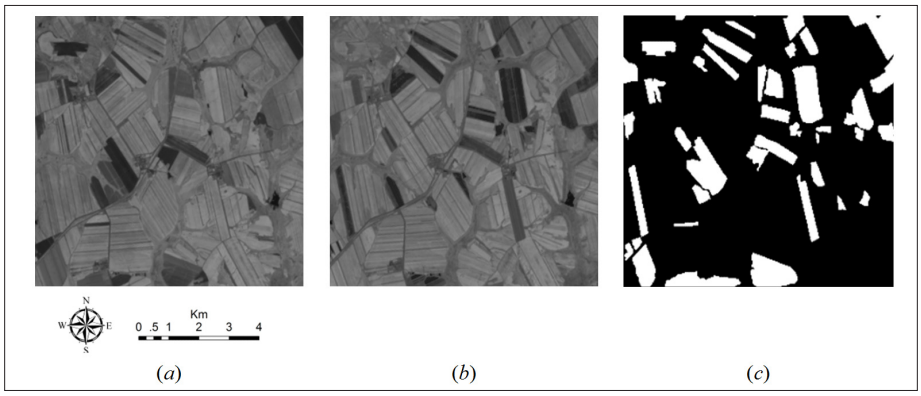


**Figure 3 - Band 4 of data set 1 (the centre coordinate: 48° 3′ N, 126° 8′ E) acquired by Landsat 7 ETM+ sensor in (*a*) August 2001 and (*b*) August 2002, (*c*) ground reference map.**

Figure 4a-f show the change detection results derived from the MLS, MLSK, FCM, EM+MRF, FCM+MRF and CSP, respectively. In MLS and MLSK, the value of parameter $\mu$ was set to 0.2, and the values of parameter $\beta$ in EM+MRF, FCM+MRF and CSP were set 1.8, 1.5 and 1.5, respectively. Additionally, the $\alpha$ of CSP was set 0.15. MLS, MLSK and FCM all obtained change maps close to the ground reference, while some "salt and pepper" noise existed in large change blocks (i.e., circle regions of Figure 4a-c). Figure 4d generated

more homogenous regions than the above three methods, some detailed information was ignored and over-smooth result was obtained (i.e. circle region). Though FCM+MRF and CSP both produced similar change map with the ground reference, the former one had some over-smooth result as shown the circle region of Figure 4e. However, CSP not only obtained homogenous regions but also preserved detailed change information instead of over-smooth results using the traditional MRF as shown in regions of Figure 4f. Table 1 lists the comparisons between false alarm, miss detection and total error of MLS, MLSK, FCM, EM+MRF, FCM+MRF and CSP. As can be seen from Table 1, CSP generated the most accurate result than other methods. This is because contrast penalty coefficients were used for different pixels in unchanged, uncertainty and changed regions, respectively, and the spatial context information was used properly without overuse.

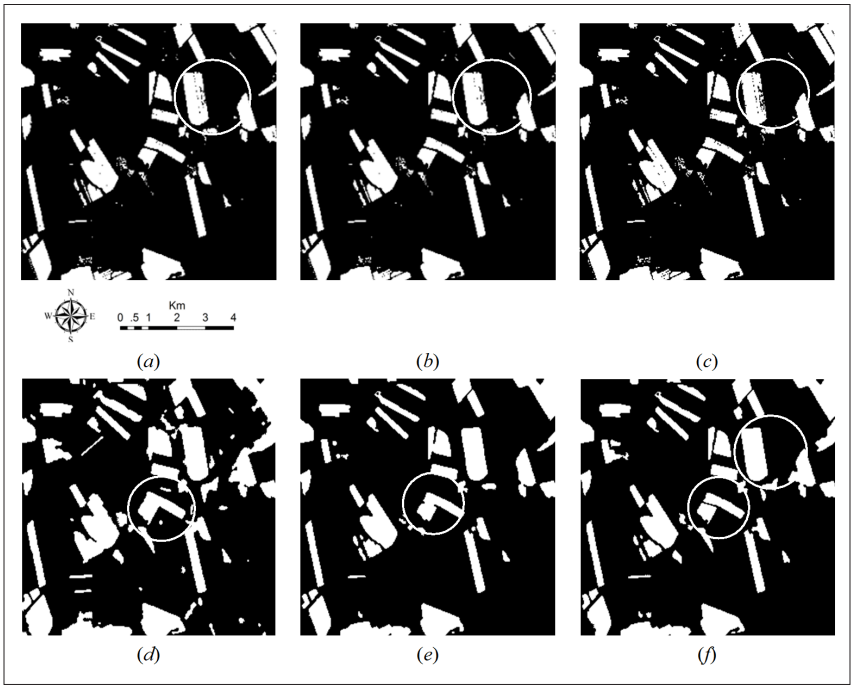


**Figure 4 - Change detection results of data set 1 obtained by (*a*) MLS, (*b*) MLSK, (*c*) FCM, (*d*) EM+MRF, (*e*) FCM+MRF and (*f*) CSP.**

**Table 1 - Quantitative change detection results of experiment 1.**

| Method | False Alarms | | Missed detections | | Total Errors | |
|---|---|---|---|---|---|---|
| | No. of pixels | $P_f$ (%) | No. of pixels | $P_m$ (%) | No. of pixels | $P_t$ (%) |
| MLS | 722 | 1.1 | 3086 | 18.7 | 3808 | 4.5 |
| MLSK | 721 | 1.1 | 3054 | 18.6 | 3775 | 4.5 |
| FCM | 669 | 1.0 | 3294 | 20.0 | 3963 | 4.7 |
| EM+MRF | 4202 | 6.2 | 725 | 4.4 | 4927 | 5.8 |
| FCM+MRF | 883 | 1.3 | 2253 | 13.7 | 3136 | 3.7 |
| CSP | 1136 | 1.7 | 1694 | 10.3 | 2830 | 3.4 |

Table 2 shows the results of proposed method using different $\alpha$ values but same $\beta$ value of 1.5. As can be seen, for the false alarm, it generally decreases as the $\alpha$ increases, and the miss detection grows with the increase of $\alpha$. Both the false alarm and miss detection change obviously at the $\alpha$ value of 0.4. However, the total error always changes slightly as the $\alpha$ grows, and all the results are more accurate than the one of traditional Potts model show in Table 1. Therefore, the proposed CSP can reduce the ignorance of significant details and excessively homogenous patches to some extent.

**Table 2 - Quantitative results of experiment 1 under different $\alpha$ values.**

| $\alpha$ | False Alarms | | Missed detections | | Total Errors | |
|---|---|---|---|---|---|---|
| | No. of pixels | $P_f$ (%) | No. of pixels | $P_m$ (%) | No. of pixels | $P_t$ (%) |
| 0.1 | 1216 | 1.8 | 1678 | 10.1 | 2869 | 3.4 |
| 0.15 | 1136 | 1.7 | 1694 | 10.3 | 2830 | 3.4 |
| 0.2 | 1146 | 1.7 | 1692 | 10.3 | 2838 | 3.4 |
| 0.3 | 1134 | 1.7 | 1696 | 10.3 | 2830 | 3.4 |
| 0.4 | 1087 | 1.6 | 1756 | 10.7 | 2843 | 3.4 |

***Experiment on the data set 2***

In the second experiment, two temporal images (400×400 pixels) in Alaska were utilized, which were acquired by the Landsat 5 Thematic Mapper (TM) sensor in July 1985 ($t_1$) and July 2005 ($t_2$). Figure 5a and 5b shows the band 4 of the multitemporal images, respectively. Then the $t_1$ image was registered to the $t_2$ image, and the histogram matching method was then applied to $t_1$ image by referencing $t_2$ image for the relative radiometric correction. The difference image was generated from all bands except band 6 using CVA method. The ground reference shown in Figure 5c was created by the manual analysis of the two temporal images.

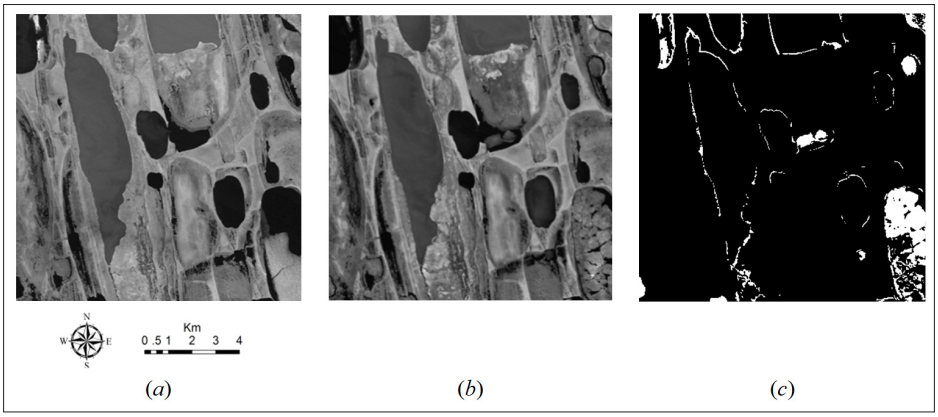


**Figure 5 - Band 4 of data set 2 (the centre coordinate: 70° 2′ N, 152° 8′ W) acquired by Landsat-5 TM sensor on (*a*) August 2001 and (*b*) August 2002, (*c*) ground reference map.**

Figure 6a-f show the change detection results derived from the MLS, MLSK, FCM, EM+MRF, FCM+MRF and CSP, respectively. In MLS and MLSK, the value of parameter $\mu$ is also set to 0.2, and the values of parameter $\beta$ in EM+MRF, FCM+MRF and CSP

are set 1.5, 0.6 and 0.6, respectively. As can be seen from Figure 6a-c, MLS, MLSK and FCM all lost so much detailed change information (i.e. circle regions) in the results. Figure 6d produced more homogenous regions than the above three methods and removed some noise; however, it lost some detailed information and yielded over-smooth results (i.e. circle region). As can be seen, FCM+MRF generated a change map similar with the one of CSP, but it lost some detailed information as shown in circle region of Figure 6e. Compared with FCM+MRF, CSP gave a more satisfactory change detection result, shown in circle regions of Figure 6f; it not only yielded more homogenous regions but preserved detailed change information, reducing the oversmooth of MRF. Table 3 lists the comparison of false alarm, miss detection and total error of MLS, MLSK, FCM, EM+MRF, FCM+MRF and CSP. As can be seen from Table 3, CSP yielded the highest change detection accuracy than other methods used in this paper. The reason is that the spatial context information is exploited properly by introducing contrast penalty coefficients for pixels in unchanged, uncertainty and changed regions instead of equivalent penalty coefficient of spatial energy term.

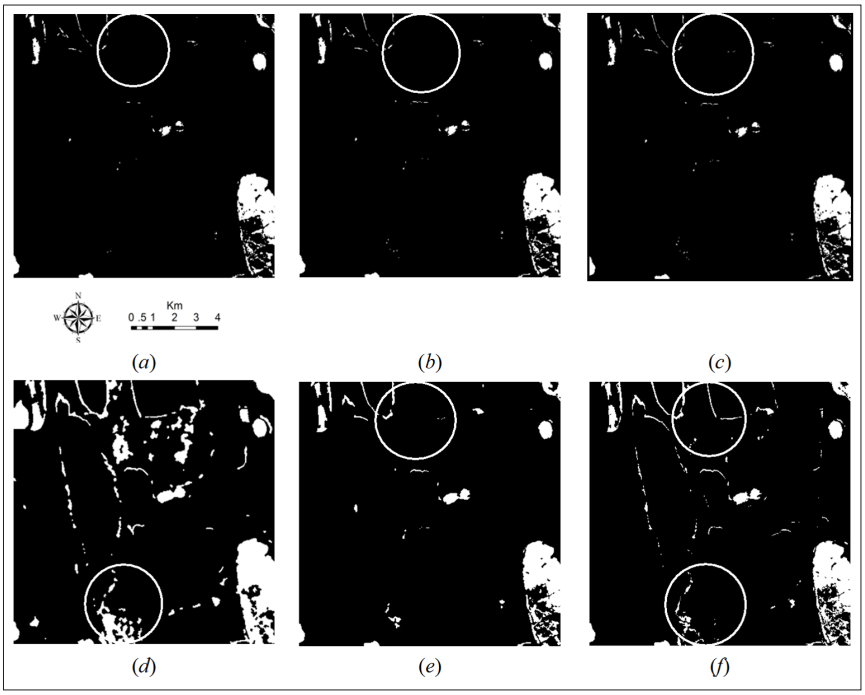


**Figure 6 - Change detection results of data set 2 yielded by (*a*) MLS, (*b*) MLSK, (*c*) FCM, (*d*) EM+MRF, (*e*) FCM+MRF and (*f*) CSP.**

Table 4 displays the results of proposed CSP method under different $\alpha$ values but same $\beta$ value of 0.6. Generally, the false alarm increases but the miss detection decrease as the $\alpha$ grows. The total error changes slightly when the $\alpha$ ranges from 0.1 to 0.3, which indicates the proposed method is robust to the parameter $\alpha$ to some extent. Though the total error has an obvious increase at the $\alpha$ value of 0.4, the proposed CSP approach often generates more accurate results than the one of traditional Potts model.

**Table 3 - Quantitative change detection results of experiment 2.**

| Method | False Alarms | | Missed detections | | Total Errors | |
|---|---|---|---|---|---|---|
| | No. of pixels | $P_f$ (%) | No. of pixels | $P_m$ (%) | No. of pixels | $P_t$ (%) |
| MLS | 128 | 0.1 | 3639 | 37.4 | 3767 | 2.4 |
| MLSK | 138 | 0.1 | 3597 | 36.9 | 3735 | 2.3 |
| FCM | 118 | 0.1 | 3595 | 36.9 | 3713 | 2.3 |
| EM+MRF | 9042 | 6.0 | 449 | 4.6 | 9491 | 5.9 |
| FCM+MRF | 781 | 0.5 | 2005 | 20.5 | 2786 | 1.7 |
| CSP | 1276 | 0.9 | 905 | 9.3 | 2181 | 1.4 |

**Table 4 - Quantitative results of experiment 2 under different $\alpha$ values.**

| $\alpha$ | False Alarms | | Missed detections | | Total Errors | |
|---|---|---|---|---|---|---|
| | No. of pixels | $P_f$ (%) | No. of pixels | $P_m$ (%) | No. of pixels | $P_t$ (%) |
| 0.1 | 1283 | 0.9 | 892 | 9.2 | 2175 | 1.4 |
| 0.15 | 1276 | 0.9 | 905 | 9.3 | 2181 | 1.4 |
| 0.2 | 1276 | 0.9 | 905 | 9.3 | 2181 | 1.4 |
| 0.3 | 1285 | 0.9 | 901 | 9.3 | 2186 | 1.4 |
| 0.4 | 1197 | 0.8 | 1044 | 10.7 | 2241 | 1.4 |

In short, the proposed contrast-sensitive Potts model based on the unchanged, uncertainty and changed regions of difference image outperforms MLS, MLSK, FCM, EM+MRF, and FCM+MRF with equivalent penalty coefficients in terms of total error. Experimental results indicate that the CSP approach is competitive and often performs more accurately than the other methods used in this paper.

## Conclusions

In this paper, a contrast-sensitive Potts model custom-designed for change detection approach is presented. First, the difference image is generated using CVA method, and then FCM preliminarily partitions the difference image into unchanged and changed clusters, in which the initial result and some parameters (i.e. center and middle pixels) are prepared for CSP. Second, the difference is divided into unchanged, uncertainty and changed regions using gray values of pixels, and different strategies are then proposed for pixels in different regions to obtain contrast penalty coefficients of the spatial energy term in Potts model of MRF. The CSP contributes the appropriate penalty coefficients of spatial context information, and reduces the over-smooth risk to a certain extent. Finally, after obtaining the contrast penalty coefficients, MRF with contrast-sensitive Potts model is run to obtain the final change map. Experimental results indicate that CSP often yields more accurate results than other methods used in this paper. Therefore, CSP is an effective approach to unsupervised change detection for optical satellite images.

## Acknowledgement

The work is supported by the Fundamental Research Funds for the Central Universities under Grant 2012LWB31 and A Project Funded by the Priority Academic Program Development of Jiangsu Higher Education Institutions.

## References

Bazi Y., Melgani F., Al-Sharari H.D. (2010) - *Unsupervised change detection in multispectral remotely sensed imagery with level set methods.* IEEE Transactions on Geoscience and Remote Sensing, 48: 3178-3187. doi: http://dx.doi.org/10.1109/tgrs.2010.2045506.

Bezdek J.C., Ehrlich R., Full W. (1984) - *FCM: The fuzzy c-means clustering algorithm*. Computers & Geosciences, 10: 191-203. doi: http://dx.doi.org/10.1016/0098-3004(84)90020-7.

Bruzzone L., Bovolo F. (2013) - *A Novel Framework for the Design of Change-Detection Systems for Very-High-Resolution Remote Sensing Images*. Proceedings of the IEEE, 101: 609-630. doi: http://dx.doi.org/10.1109/jproc.2012.2197169.

Bruzzone L., Prieto D.F. (2000) - *Automatic analysis of the difference image for unsupervised change detection*. IEEE Transactions on Geoscience and Remote Sensing, 38: 1171-1182. doi: http://dx.doi.org/10.1109/36.843009.

Chen J., Gong P., He C.Y., Pu R.L., Shi P.J. (2003) - *Land-use/land-cover change detection using improved change-vector analysis*. Photogrammetric Engineering and Remote Sensing, 69: 369-379. wos: 000221193000006.

Chen W., Moriya K., Sakai T., Koyama L., Cao C.X. (2014) - *Monitoring of post-fire forest recovery under different restoration modes based on time series Landsat data.* European Journal of Remote Sensing, 47: 153-168. doi: http://dx.doi.org/10.5721/EuJRS20144710.

Du P., Liu S., Gamba P., Tan K., Xia J. (2012) - *Fusion of Difference Images for Change Detection Over Urban Areas*. IEEE Journal of Selected Topics in Applied Earth Observations and Remote Sensing, 5: 1076-1086. doi: http://dx.doi.org/10.1109/jstars.2012.2200879.

Ghosh A., Subudhi B.N., Ghosh S. (2012) - *Object Detection From Videos Captured by Moving Camera by Fuzzy Edge Incorporated Markov Random Field and Local Histogram Matching*. IEEE Transactions on Circuits and Systems for Video Technology, 22: 1127-1135. doi: http://dx.doi.org/10.1109/tcsvt.2012.2190476.

Hao M., Shi W.Z., Zhang H., Li C. (2014) - *Unsupervised Change Detection With Expectation-Maximization-Based Level Set*. IEEE Geoscience and Remote Sensing Letters, 11: 210-214. doi: http://dx.doi.org/10.1109/lgrs.2013.2252879.

Mari N., Laneve G., Cadau E., Porcasi X. (2012) - *Fire Damage Assessment in Sardinia: the use of ALOS/PALSAR data for post fire effects management*. European Journal of Remote Sensing, 45: 233-241. doi: http://dx.doi.org/10.5721/EuJRS20124521.

Shi W.Z., Hao M. (2013) - *A method to detect earthquake-collapsed buildings from high-resolution satellite images*. Remote Sensing Letters, 4: 1166-1175. doi: http://dx.doi.org/10.1080/2150704x.2013.858839.

Solberg A.H.S., Taxt T., Jain A.K. (1996) - *A Markov random field model for classification of multisource satellite imagery*. IEEE Transactions on Geoscience and Remote Sensing, 34: 100-113. doi: http://dx.doi.org/10.1109/36.481897.

Tarabalka Y., Fauvel M., Chanussot J., Benediktsson J.A. (2010) - *SVM- and MRF-Based Method for Accurate Classification of Hyperspectral Images*. IEEE Geoscience and Remote Sensing Letters, 7: 736-740. doi: http://dx.doi.org/10.1109/lgrs.2010.2047711.

Tso B., Olsen R.C. (2005) - *A contextual classification scheme based on MRF model with improved parameter estimation and multiscale fuzzy line process*. Remote Sensing of

Environment, 97: 127-136. doi: http://dx.doi.org/10.1016/j.rse.2005.04.021.

Xiong B.L., Chen Q., Jiang Y.M., Kuang G.Y. (2012) - *A threshold selection method using two sar change detection measures based on the Markov random field model*. IEEE Geoscience and Remote Sensing Letters, 9: 287-291. doi: http://dx.doi.org/10.1109/lgrs.2011.2166149.

Zhang P.L., Lv Z.Y., Shi W.Z. (2014) - *Local Spectrum-Trend Similarity Approach for Detecting Land-Cover Change by Using SPOT-5 Satellite Images*. IEEE Geoscience and Remote Sensing Letters, 11: 738-742. doi: http://dx.doi.org/10.1109/lgrs.2013.2278205.